Article

Cell Reports

MTAP Deletions in Cancer Create Vulnerability to Targeting of the MAT2A/PRMT5/RIOK1 Axis

Graphical Abstract

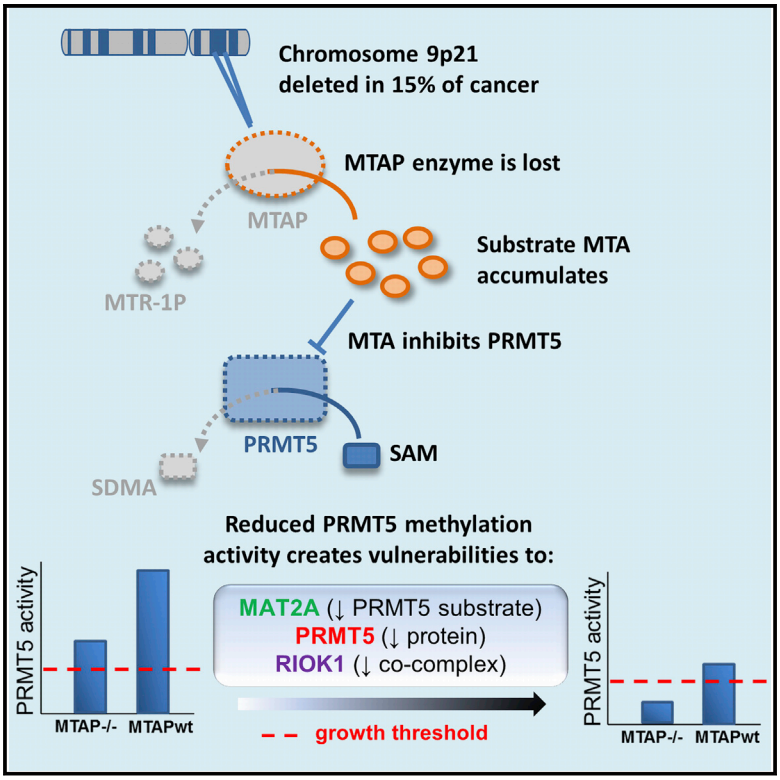

Highlights

- *MTAP* is adjacent to the *CDKN2A* tumor suppressor and is often deleted in cancer
- A genetic screen reveals genes that show synthetic lethality with *MTAP* deletion
- Metabolite accumulation in MTAP-null cancers creates sensitivity to PRMT5 targeting
- This vulnerability extends to the upstream and downstream enzymes, MAT2A and RIOK1

Authors

Katya Marjon, Michael J. Cameron, Phong Quang, ..., Marion Dorsch, Scott A. Biller, Kevin M. Marks

Correspondence

kevin.marks@agios.com

In Brief

Marjon et al. show that multiple synthetic lethal targets emerge in cancers with *MTAP* deletion. MTAP loss leads to the accumulation of its substrate, which inhibits the activity of the methyltransferase PRMT5 and sensitizes cancer cells to PRMT5 targeting. Enzymes supporting PRMT5 function, including MAT2A and PRMT5 binding partner, RIOK1, are also vulnerable.

Marjon et al., 2016, Cell Reports *15*, 574–587
April 19, 2016
http://dx.doi.org/10.1016/j.celrep.2016.03.043

OPEN ACCESS
CellPress

Cell Reports
Article

MTAP Deletions in Cancer Create Vulnerability to Targeting of the MAT2A/PRMT5/RIOK1 Axis

Katya Marjon,[1] Michael J. Cameron,[1] Phong Quang,[1] Michelle F. Clasquin,[1] Everton Mandley,[1] Kaiko Kunii,[1,3] Michael McVay,[1] Sung Choe,[1] Andrew Kernytsky,[1,2] Stefan Gross,[1] Zenon Konteatis,[1] Joshua Murtie,[1] Michelle L. Blake,[1,4] Jeremy Travins,[1] Marion Dorsch,[1] Scott A. Biller,[1] and Kevin M. Marks[1,*]

[1]Agios Pharmaceuticals, 88 Sidney Street, Cambridge, MA 02139, USA
[2]Present address: CRISPR Therapeutics, 200 Sidney Street, Cambridge, MA 02139, USA
[3]Present address: H3 Biomedicine Inc., 300 Technology Square, suite 5, Cambridge, MA 02139, USA
[4]Present address: Seattle Genetics, 21823 30th Drive SE, Bothell, WA 98021, USA
*Correspondence: kevin.marks@agios.com
http://dx.doi.org/10.1016/j.celrep.2016.03.043

SUMMARY

Homozygous deletions of p16/*CDKN2A* are prevalent in cancer, and these mutations commonly involve co-deletion of adjacent genes, including methylthioadenosine phosphorylase (*MTAP*). Here, we used shRNA screening and identified the metabolic enzyme, methionine adenosyltransferase II alpha (MAT2A), and the arginine methyltransferase, PRMT5, as vulnerable enzymes in cells with *MTAP* deletion. Metabolomic and biochemical studies revealed a mechanistic basis for this synthetic lethality. The MTAP substrate methylthioadenosine (MTA) accumulates upon MTAP loss. Biochemical profiling of a methyltransferase enzyme panel revealed that MTA is a potent and selective inhibitor of PRMT5. *MTAP*-deleted cells have reduced PRMT5 methylation activity and increased sensitivity to PRMT5 depletion. MAT2A produces the PRMT5 substrate S-adenosylmethionine (SAM), and MAT2A depletion reduces growth and PRMT5 methylation activity selectively in *MTAP*-deleted cells. Furthermore, this vulnerability extends to PRMT5 co-complex proteins such as RIOK1. Thus, the unique biochemical features of PRMT5 create an axis of targets vulnerable in *CDKN2A/MTAP*-deleted cancers.

INTRODUCTION

Loss-of-function mutations in tumor suppressor genes are critical in the molecular pathogenesis of cancer, yet few therapies selectively target cancers based on loss-of-function mutations in tumor suppressors (Lord et al., 2015). This discord can be explained by the simple observation that the mutant protein cannot be directly inhibited for therapeutic benefit. Tumor suppressors that are inactivated by homozygous deletion are most problematic for targeted therapy, because the lack of residual protein obviates therapeutic strategies that would directly activate, stabilize, or repair the defective tumor suppressor.

The chromosome 9p21 (chr9p21) locus is homozygously deleted in approximately 15% of all human cancers (Beroukhim et al., 2010), ranging in frequency up to >50% in glioblastoma multiforme (Parsons et al., 2008). The chr9p21 locus includes the *CDKN2A* gene, which encodes critical tumor suppressors p19-ARF and p16-INK4a (Figure 1A) (Kamijo et al., 1997; Serrano et al., 1993). Although chr9p21 deletion was first discovered more than 30 years ago (Chilcote et al., 1985), molecularly targeted therapies for *CDKN2A* loss have proven elusive, and it may be necessary to identify alternative approaches to target tumors with deletion of chr9p21. The chr9p21 deletions frequently involve co-deletion of genes proximal to *CDKN2A*. Foremost among these is the methylthioadenosine phosphorylase (*MTAP*) gene, which resides within 100 kb of *CDKN2A* (Figure 1A), and homozygous co-deletion of *MTAP* occurs in 80%–90% of tumors with *CDKN2A* deletion (Zhang et al., 1996). MTAP is a critical enzyme in the methionine salvage pathway that metabolizes the byproduct of polyamine synthesis, 5′-methylthioadenosine (MTA), leading to the eventual regeneration of methionine and adenine (Zappia et al., 1988). Elaboration of *MTAP*-selective anti-cancer targets remains an intriguing and unsolved scientific question (Muller et al., 2015). *MTAP* deletion has been reported to create sensitivity to inhibitors of purine biosynthesis (Li et al., 2004), although this metabolic vulnerability is lost in vivo, as tumors uptake circulating adenine and escape the purine biosynthesis sensitivity (Ruefli-Brasse et al., 2011). Despite the limited success to date in selectively targeting MTAP-deficient cancers, deletion of other metabolic genes has been shown to create targetable vulnerabilities (Frezza et al., 2011; Muller et al., 2012); thus, we sought to identify collateral vulnerabilities in MTAP-deficient cells.

To identify vulnerabilities that arise upon *MTAP* loss in cancer, we employed small hairpin RNA (shRNA) depletion screening in an isogenic cancer cell line pair that varies only in *MTAP* status. Although *MTAP* encodes a metabolic enzyme, we hypothesized that *MTAP* loss may create collateral vulnerabilities in biologic pathways that extend beyond metabolism. To test the

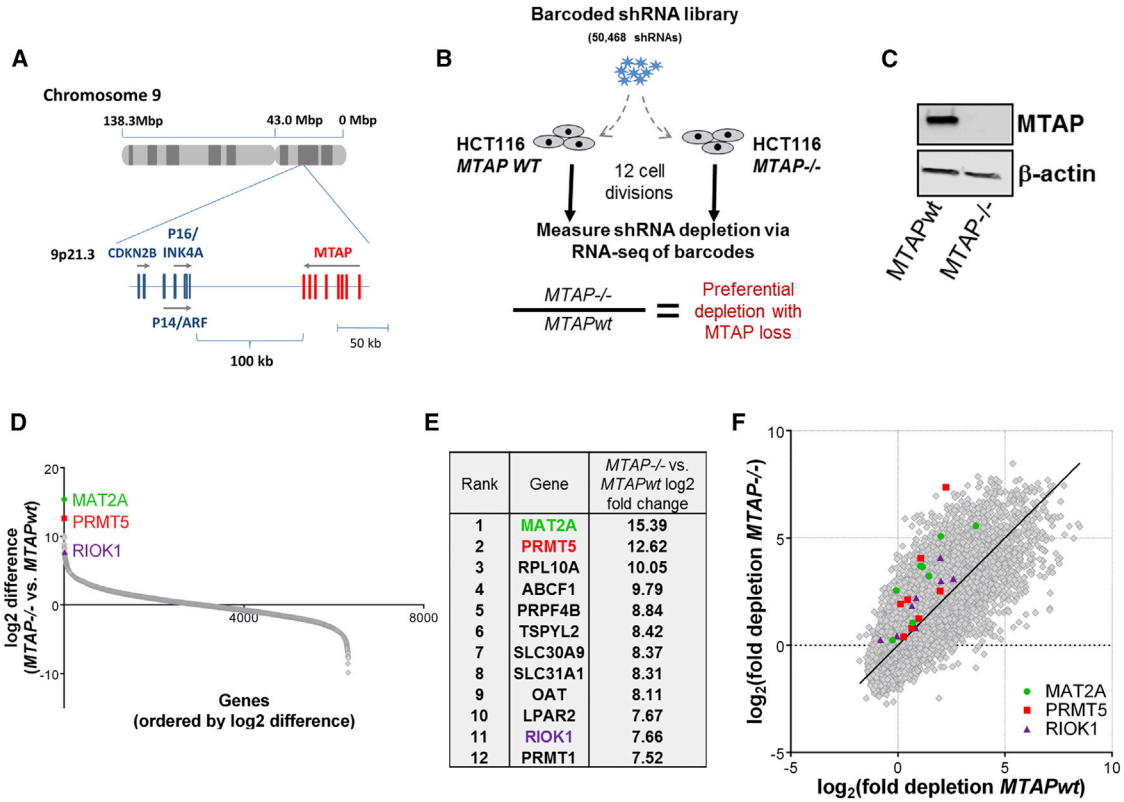

Rank	Gene	*MTAP-/-* vs. *MTAPwt* log2 fold change
1	MAT2A	15.39
2	PRMT5	12.62
3	RPL10A	10.05
4	ABCF1	9.79
5	PRPF4B	8.84
6	TSPYL2	8.42
7	SLC30A9	8.37
8	SLC31A1	8.31
9	OAT	8.11
10	LPAR2	7.67
11	RIOK1	7.66
12	PRMT1	7.52

Figure 1. Functional Genomics Screening Identifies Genes that Are Synthetic Lethal with MTAP Loss

(A) Schematic depicting the chr9 and chr9p21.3 region containing the *MTAP* gene close to the *CDKN2A* gene and its two coding sequences, *p16/INK4A* and *p19/ARF*.

(B) Schematic depicting the shRNA depletion screen in the colon carcinoma HCT116 *MTAPwt* and *MTAP*$^{-/-}$ isogenic cell line pair.

(C) Immunoblot analysis demonstrating a lack of MTAP protein expression in HCT116 *MTAP*$^{-/-}$ cells.

(D) Gene scores in HCT116 *MTAP*$^{-/-}$ versus *MTAPwt* cells.

(E) Top genes that scored as differentially depleted in HCT116 *MTAP*$^{-/-}$ cells. Genes pursued in subsequent studies are highlighted in green (*MAT2A*), red (*PRMT5*), and magenta (*RIOK1*).

(F) Changes in the abundance of the individual MAT2A, PRMT5, and RIOK1 shRNAs in HCT116 *MTAP*$^{-/-}$ versus *MTAPwt* cells in the screen. Individual shRNAs are highlighted in green (MAT2A), red (PRMT5), or magenta (RIOK1). The rest of the shRNAs in the library are shown as gray diamonds.

hypothesis that *MTAP* deletion would create collateral vulnerabilities in metabolic and non-metabolic pathways, we used a novel shRNA library consisting of shRNA hairpins targeting the 3,000+ genes of the metabolome, as well as an additional 3,000+ non-metabolic genes.

Through this screen and subsequent investigation, we identified an axis of targets that becomes vulnerable upon MTAP loss in cancer. Central in this axis is protein arginine methyltransferase 5 (PRMT5). Using metabolomic and biochemical approaches, we discovered that MTA, the substrate of the MTAP enzyme reaction, accumulates dramatically in *MTAP*-deleted cancers. MTA inhibits PRMT5 enzyme activity and leads to reduced basal PRMT5 methylation in *MTAP*-deleted cancers. This vulnerability extends both upstream and downstream of PRMT5. We show that the metabolic enzyme methionine adenosyltransferase II alpha (MAT2A), which produces PRMT5 substrate S-adenosylmethionine (SAM), is also selectively essential in *MTAP*-deleted cancers, as are multiple different PRMT5 binding partners, including the kinase RIOK1.

RESULTS

shRNA Depletion Screen in the HCT116 *MTAPwt/MTAP*$^{-/-}$ Isogenic Pair

To identify genes for which loss of function would lead to selective killing of *MTAP*-deficient cells, we performed an shRNA-based depletion screen in the HCT116 colon carcinoma cell line and an isogenic clone of HCT116 cells that had been genetically modified to delete exon 6 of the *MTAP* gene (Figure 1B), which led to complete loss of MTAP protein expression (Figure 1C). To provide broad coverage for potential synthetic lethal interactions, we constructed a library that encompassed the complete metabolome (3,067 genes), the mitochondrial proteome (Pagliarini et al., 2008), the epigenome (Arrowsmith et al., 2012), the kinome (http://www.uniprot.org/), and >1,500 additional genes representing diverse biologic pathways. HCT116 *MTAP*$^{-/-}$ and *MTAP* wild-type (WT) cells were transduced with the shRNA library containing eight shRNAs per gene, and the pool of knockdown cells was passaged for 12 cell divisions. At

the end of the culture, we measured the relative abundance of each shRNA barcode via deep sequencing and calculated the fold depletion of each shRNA compared to the untransduced library DNA. After normalization, we then calculated an *MTAP* selectivity score for each gene based on the difference in the $\log_2$ fold change in the abundance of each of the eight shRNAs targeting the gene in *MTAP*$^{-/-}$ versus *MTAPwt* cells (Figure 1D).

This analysis demonstrated that although most genes, as well as shRNA controls, had a similar score in both *MTAP*$^{-/-}$ and *MTAPwt* cells (Figure 1D), a subset of genes was selectively depleted in *MTAP*$^{-/-}$ cells (Figures 1D–1F and S1A–S1C; Table S1). The top hit in the screen was *MAT2A* (Figures 1D and 1E). MAT2A catalyzes the synthesis of the universal biologic donor of methyl groups, SAM, via adenosylation of methionine. Six of eight (75%) *MAT2A*-targeting hairpins displayed markedly increased depletion in the *MTAP*$^{-/-}$ cells compared to *MTAPwt* cells (Figures 1F and S1A). The remaining two hairpins displayed little depletion in either cell line, perhaps due to ineffective knockdown of the target. The second-best scoring gene in the screen was *PRMT5*, which is the catalytic subunit of a multiprotein methyltransferase complex that includes PRMT5 in complex with obligate binding partner WD45/MEP50 (WD repeat domain 45/methylosome protein 50), and other scaffolding proteins (Figures 1D–1F and S1B) (Meister et al., 2001; Pesiridis et al., 2009). PRMT5 belongs to the type II PRMT subfamily of arginine methyltransferases and catalyzes the formation of symmetric di-methylarginines (SDMAs) in target proteins, using MAT2A product SAM. The eleventh-highest-scoring gene, *RIOK1*, encodes a Rio domain-containing protein, which is a binding partner of PRMT5 that directs PRMT5 toward selective methylation of a subset of PRMT5 substrates (Figures 1D–1F and S1C) (Guderian et al., 2011). These data suggest that MAT2A-, PRMT5-, and RIOK1-catalyzed reactions are critical for maintaining viability of MTAP-deficient cells. Although all three highlighted hits represent therapeutically and biologically interesting targets, we first tested whether MAT2A, the top hit in our shRNA screen, represents a bona fide synthetic lethal target in MTAP-deficient cells.

MAT2A Is Selectively Essential in MTAP-Deficient Cells

We used the HCT116 isogenic pair and created cell lines stably expressing non-targeting (NT) shRNA and *MAT2A*-targeting shRNA, as well as cell lines that were additionally reconstituted with shRNA-resistant *MAT2A* cDNA or that expressed *MTAP* cDNA. We confirmed efficient MAT2A knockdown and MAT2A and MTAP re-expression in HCT116 cells by western blot (Figure 2A). We also confirmed that MAT2A knockdown resulted in reduced cellular levels of SAM in both HCT116 genotypes using liquid chromatography-mass spectrometry (LC-MS) analysis (Figure 2B). We then tested the impact of MAT2A knockdown in *MTAPwt* versus *MTAP*$^{-/-}$ cells in a 6-day in vitro growth assay (Figure 2C). The results were in agreement with our genomic screen. MAT2A knockdown selectively attenuated growth of *MTAP*$^{-/-}$ but not WT cells (Figure 2C). This growth defect was rescued by introduction of a shRNA-resistant *MAT2A* cDNA construct, indicating the on-target effect of the shRNA, and was partially rescued by MTAP re-expression (Figure 2C).

To investigate the in vitro-to-in vivo translation of our findings, we conducted xenograft efficacy studies with HCT116 isogenic cell lines expressing inducible *MAT2A* shRNA (shMAT2A). In these studies, tumors were allowed to form before treatment of animals with doxycycline (DOX) to assess the role of MAT2A in the proliferation of established tumors. Efficiency of MAT2A knockdown in vivo was confirmed by western blot (Figure S2A). We confirmed that MAT2A genetic ablation in vivo resulted in a similar reduction in SAM levels in HCT116 xenografts of both genotypes (Figure S2B). In accordance with our findings in vitro, MTAP-selective tumor growth reduction was observed in vivo upon MAT2A depletion by shRNA (Figure 2D). To demonstrate that this selective growth reduction was an on-target effect, we performed an expanded in vivo study with a WT *MAT2A* cDNA rescue of shMAT2A. This experiment confirmed the efficacy observed in our first in vivo study, and as with the in vitro studies, growth inhibition was rescued in the xenografts expressing a *MAT2A* cDNA (Figures S2C and S2D).

We next sought to assess sensitivity to MAT2A ablation in a cancer model that possesses an endogenous deletion at the *MTAP*/*CDKN2A* locus. Thus, we generated breast carcinoma MCF7 cell lines stably expressing NT shRNA and *MAT2A*-targeting shRNA, as well as cell lines that were additionally reconstituted with shRNA-resistant *MAT2A* cDNA. We demonstrated efficiency of MAT2A knockdown and re-expression by western blot (Figure 2E). Consistent with observations made in the HCT116 model system, MAT2A knockdown attenuated growth of MTAP-deleted MCF7 cells measured in a 7-day growth assay, while *MAT2A* cDNA reconstitution resulted in complete rescue of the growth phenotype (Figure 2F). We then tested MAT2A target dependence in vivo in an orthotopic MCF7 model and observed a robust reduction in MCF7 tumor growth upon MAT2A knockdown, which was fully reverted by expression of WT *MAT2A* cDNA (Figure 2G). Western blot confirmed reduction in MAT2A levels upon DOX treatment and maintenance of MAT2A expression in tumors expressing the *MAT2A* cDNA rescue construct (Figure 2H). In addition, MAT2A genetic ablation in MCF7 tumors in vivo resulted in reduction in SAM levels, which was rescued by the *MAT2A* cDNA (Figure S2E).

Although the MCF7 model indicates that the MAT2A vulnerability extends beyond the genetically engineered HCT116 *MTAP*$^{-/-}$ setting, we sought to test further the MTAP selectivity of MAT2A dependence by performing shRNA studies in a panel of seven additional cell lines that vary in deletion status at the endogenous *CDKN2A*/*MTAP* locus. MAT2A knockdown led to greater growth inhibition in the *CDKN2A*/*MTAP*-deleted cells (Figure 2I). MAT2A knockdown was comparable across the cell line panel, irrespective of *CDKN2A*/*MTAP* deletion status (Figure S2F). Thus, the selective vulnerability that we identified in our HCT116 model system screen persists in tumors with endogenous deletion of the *CDKN2A*/*MTAP* locus.

MTAP Deficiency Creates an Altered Metabolic State

To better understand the connection between MTAP deficiency and MAT2A function in cells, we next investigated metabolic changes that occur upon MTAP loss. Both MTAP and MAT2A participate in the reactions of the methionine pathway (Figure 3A). MAT2A generates SAM, the universal biologic donor

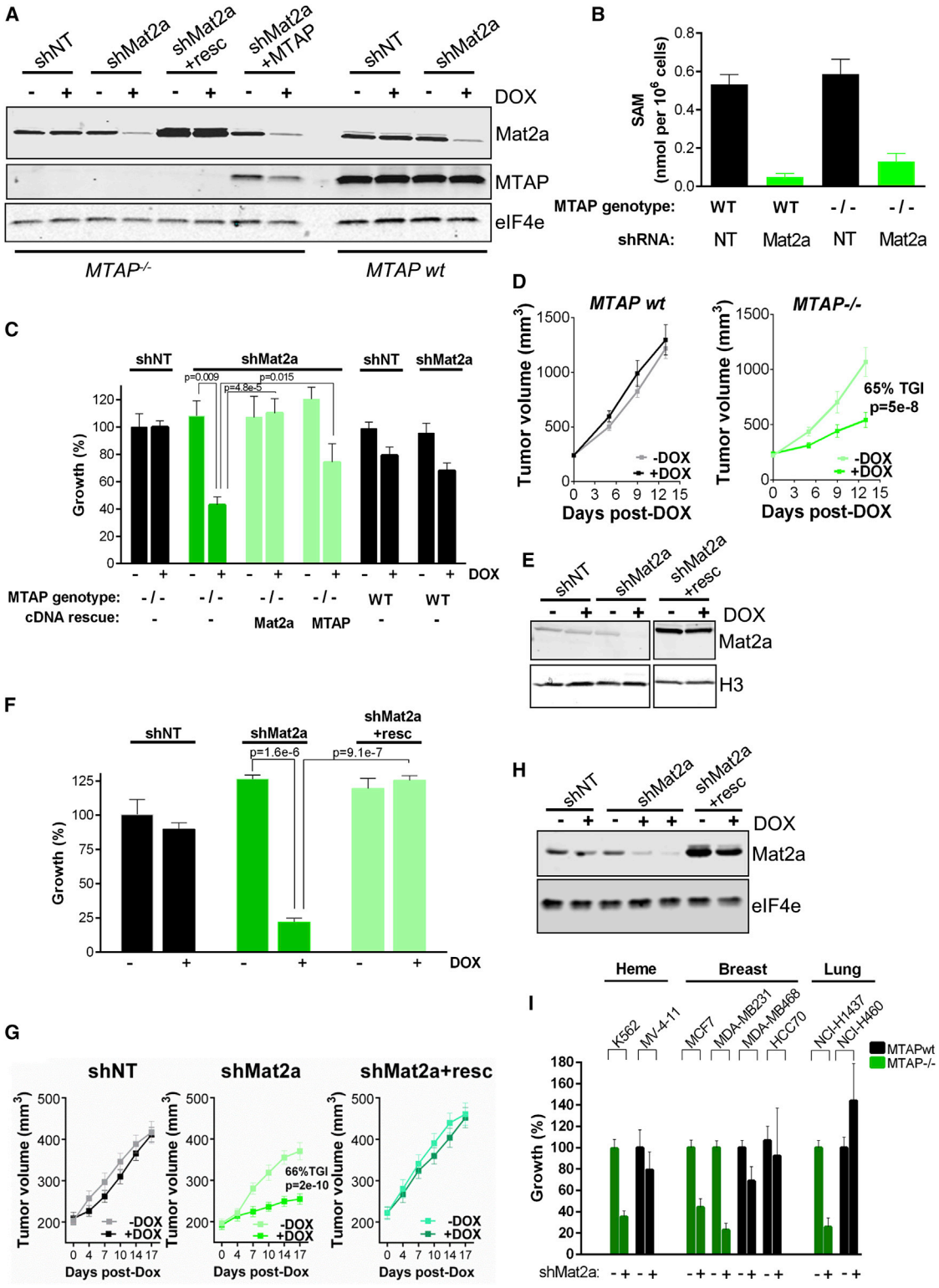

Figure 2. MAT2A Is Selectively Essential in HCT116 *MTAP*$^{-/-}$ Cells

(A) Immunoblot analysis of the indicated proteins in HCT116 *MTAP*$^{-/-}$ and *MTAPwt* cells stably expressing NT shRNA (shNT), shMAT2A, shRNA-resistant *MAT2Awt* cDNA (shMAT2A+resc), or shMAT2A and *MTAP* cDNA (shMAT2A+MTAP). DOX (200 ng/ml) was added to induce shRNA expression.

(B) SAM levels as determined by targeted LC-MS analysis in the HCT116 isogenic pair expressing inducible shNT or shMAT2A (mean ± SD, n = 3). All cells were treated with DOX.

(legend continued on next page)

of methyl groups, from ATP and methionine. MTAP converts MTA, a byproduct of polyamine biosynthesis, back to methionine and adenine in the methionine salvage pathway (Figure 3A). Because MTAP is the only enzyme in mammalian cells known to catalyze the degradation of MTA, we hypothesized that MTAP deficiency would result in accumulation of MTA and blockade of the methionine salvage pathway. We first tested this hypothesis in the context of a broad, untargeted LC-MS-based metabolomic assessment of intracellular metabolite levels in the HCT116 MTAP isogenic pair (Figure 3B). This analysis revealed that, among 237 annotated metabolites that were detected, MTA displayed the largest abundance increase in *MTAP*$^{-/-}$ cells compared to HCT116 parental control (Figure 3B, left panel). Decarboxylated S-adenosylmethionine (dcSAM), the metabolite upstream from MTA in the polyamine biosynthetic pathway, displayed the second-largest increase. The enrichment of these two metabolites in *MTAP*$^{-/-}$ cells was highly statistically significant (Figure 3B, right panel). Elevation of MTA was confirmed using absolute quantitation with targeted LC-MS analysis in the HCT116 isogenic pair (Figure 3C). A screen of a large cancer cell line panel comprising 249 cell lines of diverse tissue origin demonstrated consistent accumulation of MTA in the media of cells with endogenous *MTAP* deletion (Figure 3D), suggesting that *MTAP*$^{-/-}$ HCT116 cancer cells faithfully recapitulate the metabolic phenotype of *CDKN2A/MTAP*-deleted cells.

MTA Inhibits PRMT5 Activity In Vitro and In Vivo

MTA and structurally related analogs have been reported to inhibit a protein methyltransferase activity partially purified from chick embryos, albeit with an inhibitor constant (Ki) of 400 μM, indicating very low potency of inhibition (Enouf et al., 1979). We hypothesized that MTA might more potently and selectively inhibit specific methyltransferases, such as PRMT5. To test this hypothesis, we performed an in vitro biochemical screen assessing activity of 33 different N-methyltransferases following treatment with 10 and 100 μM MTA. Inhibition by MTA was only observed in a small subset of the panel, and strongest inhibition was observed for PRMT5 and PRMT4, members of the arginine methyltransferase family (Figure 4A). Furthermore, PRMT5 demonstrated high sensitivity to MTA in subsequent experiments testing a range of MTA concentrations (Figure 4B). Next, we analyzed the MTA Ki for PRMT5, PRMT4, and a diverse subset of methyltransferases (Figure 4C; Table S4). Strikingly, the MTA Ki for PRMT5 (0.26 μM) was >20-fold lower than that of any other methyltransferase, indicating that PRMT5 is far more sensitive to inhibition by MTA than any other methyltransferase tested. This biochemical observation is consistent with our shRNA screening data demonstrating that PRMT5 was the strongest *MTAP*$^{-/-}$ selective hit among all methyltransferases in the library (Figure 1D; Table S1).

We next assessed whether MTA accumulation in MTAP-deficient cells reduces PRMT5 activity. We performed western blot analysis of SDMA marks in total cell lysates of a panel of *MTAPwt* and *MTAP*-deleted cell lines, using an antibody that was generated using symmetric dimethyl histone H4R3 antigen and detects multiple SDMA marks (Figure 4D). We observed that *MTAP*-deleted cell lines consistently demonstrated lower levels of SDMA marks. Finally, we took advantage of the availability of a potent, cell permeable transition state analog inhibitor of MTAP (Basu et al., 2011; Longshaw et al., 2010). We treated HCT116 *MTAPwt* cells with the MTAP inhibitor for 3 days and measured the impact of pharmacologic inhibition of MTAP on the levels of SDMA marks (Figure 4E). Treatment of *MTAPwt* cells with MTAP inhibitor at doses sufficient to increase MTA levels to those observed in *MTAP*$^{-/-}$ cells (Figure S4A) resulted in reduction in the levels of SDMA marks (Figure 4E) without an impact on cell growth (Figure S4B). The reduction observed upon pharmacologic inhibition of MTAP was equivalent to that observed upon genetic deletion of *MTAP*. These data strongly indicate that PRMT5 activity is impaired by MTA in *MTAP*-deleted cells, resulting in reduced methylation of its protein substrates. Because PRMT5 was a top hit in the shRNA screen, we hypothesized that reduced basal activity of PRMT5 upon MTAP loss creates vulnerability to additional ablation of PRMT5 activity by shRNA.

PRMT5 Is Selectively Essential in *MTAP*$^{-/-}$ Cells upon Genetic Ablation

We thus sought to confirm that PRMT5, similarly to MAT2A, represents a bona fide synthetic lethal target in MTAP-deficient cells. Initially, we performed small interfering RNA (siRNA)-mediated knockdown of PRMT5 in the HCT116 isogenic pair (Figures S5A and S5B). Four separate PRMT5-targeting siRNAs displayed a significant growth reduction in HCT116 *MTAP*$^{-/-}$ cells, with only modest impact on the growth of HCT116 *MTAPwt* cells. Furthermore, reconstitution of HCT116 *MTAP*$^{-/-}$ cells

(C) MAT2A is selectively essential in HCT116 *MTAP*$^{-/-}$ cells in vitro. Percent growth of HCT116 *MTAP*$^{-/-}$ and *MTAPwt* cells upon MAT2A knockdown (+DOX), with or without *MAT2A* or *MTAP* rescue, versus no knockdown (−DOX) control measured in a 6-day in vitro growth assay (mean ± SD, n = 5). The p values were calculated using a two-tailed paired t test.

(D) Kinetics of tumor growth upon in vivo ablation of MAT2A in subcutaneous xenografts of shMAT2A HCT116 isogenic pair cell lines. DOX treatment was initiated once tumors reached 200–300 mm^3 in diameter (mean ± SEM, n = 5–6).

(E) Immunoblot analysis of the indicated proteins in MCF7 cells stably expressing shNT, shMAT2A, and shMAT2A+resc. DOX indicates where hairpin expression was induced.

(F) MAT2A is essential in MCF7 cells in vitro. Percent growth of MCF7 cells upon MAT2A knockdown (+DOX), with or without MAT2A rescue, versus no knockdown (−DOX) control measured in a 7-day in vitro growth assay (mean ± SD, n = 5). The p values were calculated using a two-tailed paired t test.

(G) Kinetics of tumor growth upon in vivo ablation of MAT2A in orthotopic MCF7 tumors. DOX treatment was initiated once tumors reached 200–300 mm^3 in diameter (mean ± SEM, n = 9–10).

(H) Immunoblot analysis of the indicated proteins in tumors formed from MCF7 cells stably expressing shMAT2A, with or without MAT2A rescue. DOX was added to the mouse chow to induce shMAT2A expression.

(I) Cell lines were stably transduced with shMAT2A or control shRNA (shNT or Luc), and impact of MAT2A knockdown on cell growth was measured in a 6-day in vitro growth assay (mean ± SD, n = 15).

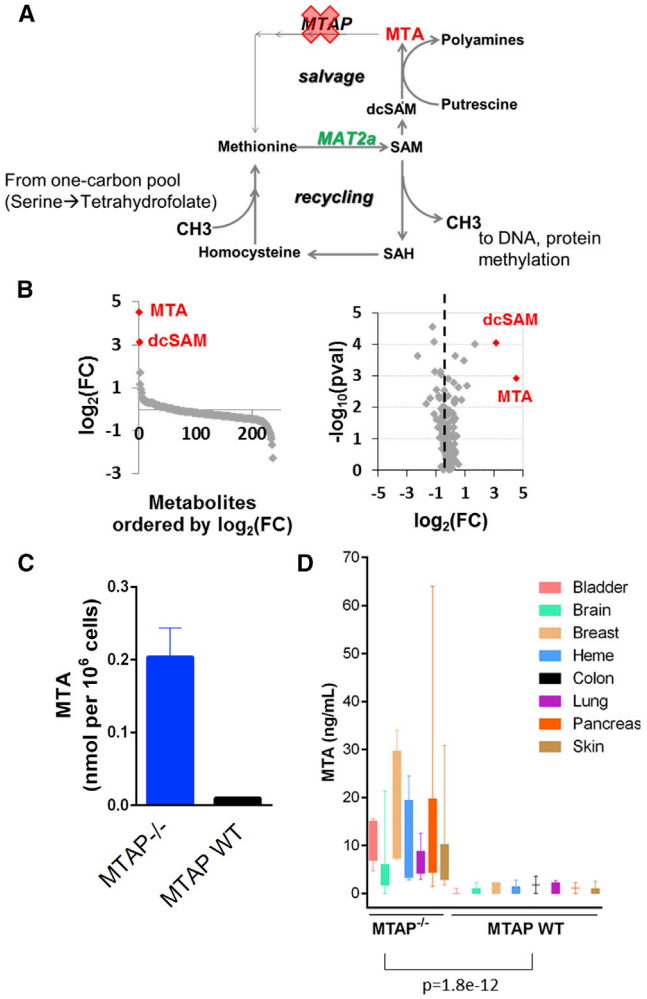

Figure 3. MTA Accumulates in MTAP-Deficient Cancers

(A) Schematic of methionine recycling and salvage pathways.

(B) Intracellular metabolite levels analysis using untargeted LC-MS in the HCT116 isogenic cell line pair. Waterfall plot demonstrates the $\log_2$ of mean fold change (FC) in HCT116 *MTAP*$^{-/-}$ cells compared with *MTAPwt* control versus metabolite identification. Volcano plot of the $\log_2$ of mean FC in HCT116 *MTAP*$^{-/-}$ cells compared with *MTAPwt* control versus $\log_{10}$ p value for each metabolite is also shown. MTA and dcSAM are highlighted in red.

(C) Measurement of intracellular MTA levels in HCT116 isogenic cell lines by targeted LC-MS (mean ± SD, n = 3).

(D) Media MTA levels in a panel of 249 cancer cell lines of various tissues of origin.

with *MTAP* cDNA resulted in attenuation of the growth phenotype upon PRMT5 knockdown (Figures S5C and S5D). We next generated HCT116 *MTAP*$^{-/-}$ and *MTAPwt* cell lines stably expressing DOX-inducible shRNA targeting *PRMT5*. We confirmed that *PRMT5* was efficiently knocked down by measuring levels of PRMT5 protein (Figure 5A). Consistent with our genomic screening results, PRMT5 knockdown with DOX-inducible shRNA led to more complete growth reduction in *MTAP*$^{-/-}$ cells than in *MTAPwt* cells (Figure 5B). Expression of a small hairpin PRMT5-resistant *PRMT5* cDNA in *MTAP*$^{-/-}$ cells rescued growth inhibition upon endogenous PRMT5 knockdown, while expression of catalytically dead R368A *PRMT5* mutant (Pollack et al., 1999) cDNA did not (Figure 5B). Thus, the anti-proliferative effect of this shRNA is due to PRMT5 depletion, not off-target shRNA effects. Lack of rescue by R368A mutant PRMT5 indicates that PRMT5 enzyme activity is essential in *MTAP*$^{-/-}$ cells. These findings provide validation of our screening results and suggest that PRMT5 catalytic function is critical for maintaining growth of MTAP-deficient cells. Because PRMT5 activity results in SDMA residues in numerous cellular proteins, we next assessed the impact of PRMT5 knockdown on SDMA marks in our model (Figure 5C). As was observed in the cell panel analysis (Figure 4D), we noted that *MTAP*$^{-/-}$ cells have lower basal levels of SDMA marks, suggesting impaired basal PRMT5 activity. Furthermore, PRMT5 knockdown led to more complete reduction in levels of SDMA marks in the *MTAP*$^{-/-}$ cell line, despite equivalent reduction in the PRMT5 protein level in *MTAP*$^{-/-}$ and WT cells. The reduction in SDMA marks was rescued by WT *PRMT5* but not by R368A mutant *PRMT5* cDNA (Figure 5C). To validate our findings, we pre-treated HCT116 *MTAPwt* cells stably expressing DOX-inducible shRNA targeting PRMT5 with MTAP inhibitor to induce MTA accumulation and reduce activity of the endogenous PRMT5 (Figures 4E and S4). We then assessed the impact of PRMT5 knockdown on the growth of HCT116 *MTAPwt* cells in the absence or presence of MTAP inhibitor (Figures 5D and 5E). Similar to the phenotype observed in *MTAP*$^{-/-}$ cells, MTAP inhibitor treatment sensitized *MTAPwt* cells to PRMT5 knockdown (Figure 5D).

A potent and selective inhibitor of PRMT5, EPZ015666, was developed recently (Chan-Penebre et al., 2015). Thus, we sought to test whether pharmacologic targeting of PRMT5 function in MTAP-deficient cells would recapitulate our finding using genetic ablation of PRMT5. Surprisingly, growth inhibition upon pharmacologic inhibition of PRMT5 with EPZ015666 was not selective for the *MTAP*$^{-/-}$ genetic background (Figure 5F). EPZ015666 treatment reduced SDMA levels in both *MTAP*$^{-/-}$ and *MTAPwt* cells, with modestly better potency in the *MTAPwt* cells (Figure 5G). We then tested the impact of EPZ015666 on the growth of a panel of 64 cell lines. Again, we did not observe differential sensitivity of *MTAP*-deleted cells to growth inhibition by EPZ015666 (Figure 5H; Table S5), indicating that the lack of selective growth inhibition with EPZ015666 is not unique to the genetically engineered HCT116 cell model. This finding was unexpected, considering that the catalytically dead mutant of PRMT5 did not rescue the growth of PRMT5 shRNA-expressing HCT116 *MTAP*$^{-/-}$ cells, which suggested that loss of PRMT5 catalytic function was necessary and sufficient for selective growth inhibition of *MTAP*$^{-/-}$ cells (Figures 5A–5C). This discrepancy between the impact of genetic and that of pharmacologic PRMT5 ablation on the growth of *MTAP*$^{-/-}$ cells led us to assess the mechanistic link between MAT2A and PRMT5 in *MTAP*$^{-/-}$ cells as a means to validate the synthetic lethal relationships between MAT2A/PRMT5 and MTAP.

MAT2A Loss Selectively Inhibits PRMT5 Activity in *MTAP*-Deleted Cells

MAT2A generates SAM, which is the universal substrate for cellular methylation reactions; thus, reduction in SAM levels upon depletion of MAT2A may affect the function of

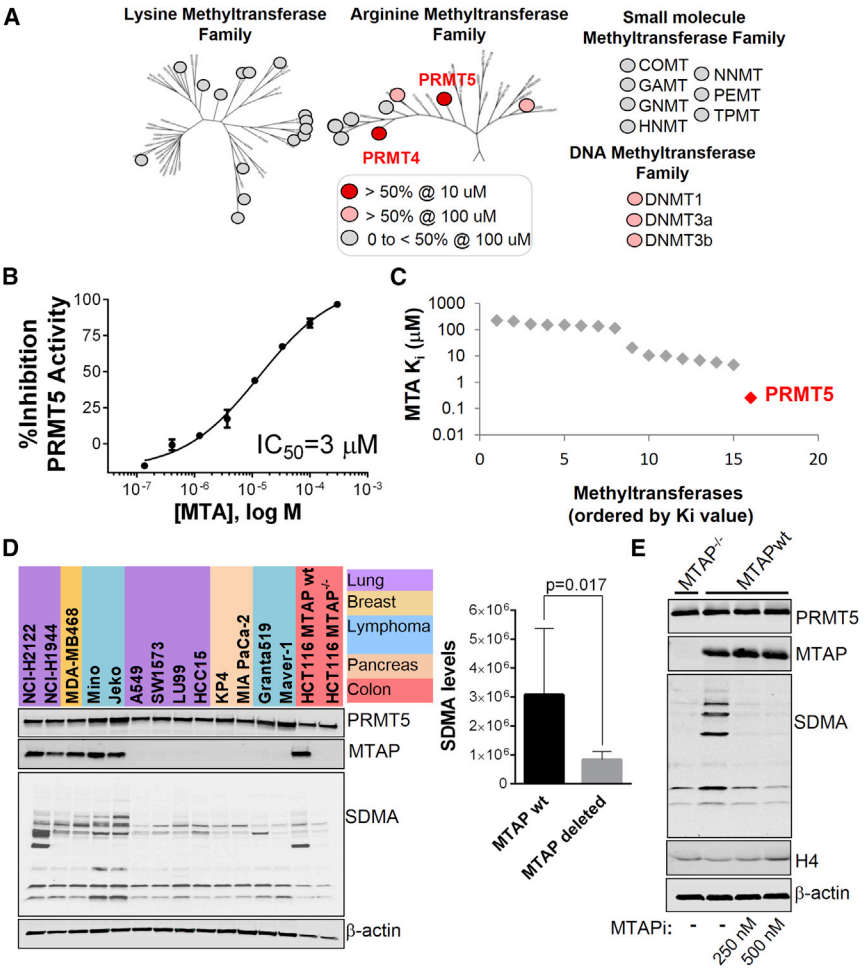

Figure 4. MTA Inhibits PRMT5 Activity In Vitro and In Vivo

(A) MTA sensitivity of a panel of N-methyltransferases. A panel of small molecule-, DNA-, lysine-, and arginine- N-methyltransferases was tested using an in vitro assay in the presence of 10 and 100 μM concentrations of MTA.

(B) Dose-response curve for MTA inhibition of PRMT5 complex activity in an in vitro assay.

(C) Waterfall plot of the MTA Ki values for a subset of N-methyltransferases. The PRMT5 data point is highlighted in red.

(D) Immunoblot analysis of the indicated proteins in a panel of *MTAPwt* and *MTAP*-deleted cancer cell lines of various tumor origin. HCT116 *MTAPwt* and *MTAP*$^{-/-}$ cell lines were included as a reference. Levels of SDMA marks were quantified using LI-COR software (value ± SD). The p value was calculated using a two-tailed unpaired t test.

(E) Immunoblot analysis of the indicated proteins in HCT116 *MTAP*$^{-/-}$ and *MTAPwt* cells treated with the MTA transition state analog inhibitor of MTAP (MTAPi) at 250 or 500 nM for 3 days.

methyltransferases, including PRMT5. To that end, we measured levels of PRMT5-dependent SDMA marks in our shMAT2A HCT116 isogenic pair. We observed a significant reduction in SDMA marks upon MAT2A knockdown in *MTAP*$^{-/-}$ cells but not *MTAPwt* cells (Figure 6A). The *MTAP*$^{-/-}$ selective reduction in PRMT5-dependent SDMA marks upon *MAT2A* knockdown was rescued in the presence of shRNA-resistant *MAT2A* or *MTAP* cDNA (Figure S6). We next tested whether MTAP pharmacologic inhibition would similarly synergize with MAT2A knockdown to reduce SDMA marks in *MTAPwt* cells. Much like genetic deletion of *MTAP*, pharmacologic inhibition of MTAP, combined with MAT2A knockdown, led to a profound reduction in SDMA marks (Figure 6B). Finally, we confirmed that MAT2A knockdown reduces SDMA marks in MCF7 cells, which possess an endogenous deletion of the *CDKN2A/MTAP* locus (Figure 6C). In combination with our observation regarding the strong inhibitory impact of MTA on PRMT5 activity, these data suggest that PRMT5 function in the *MTAP*-deleted background is highly dependent on adequate availability of SAM. PRMT5 was reported in the literature to exhibit low affinity for SAM (Antonysamy et al., 2012; Sun et al., 2011). We thus compared SAM Michaelis-Mentin constant (Km) values for the N-methyltransferases from our in vitro biochemical panel analysis and observed that PRMT5 exhibited the lowest affinity for SAM (Figure 6D). This finding may explain PRMT5 dependence on proper MAT2A function, especially in the metabolically altered, high-MTA environment of MTAP-deficient cells (Figure 6E). These data demonstrate that metabolic vulnerability due to MTAP deficiency extends upstream of PRMT5, creating dependence on the availability of PRMT5 substrate SAM and therefore the activity of SAM-producing enzyme MAT2A. In addition, we observed MAT2A sensitivity in a number of *MTAP*-deleted cancer cell lines, indicating that this selective vulnerability is a bona fide feature of cancers with deletion of chr9p21.

Multiple PRMT5 Co-Complexes Are Vulnerable in *MTAP*-Deleted Cells

The Rio domain containing protein, RIOK1, was another strong hit in our shRNA depletion screening campaign. Because it is a PRMT5 binding partner, we sought to confirm the synthetic lethal phenotype upon genetic ablation of RIOK1 in the HCT116 MTAP isogenic cells. Similar to the characterization that was performed for PRMT5 and MAT2A, inducible *RIOK1* shRNA cell lines, as well as *RIOK1wt* rescue and *RIOK1* active site (D324N) and ATP binding domain (K208R) catalytically inactive mutant (Angermayr et al., 2002; Widmann et al., 2012) cell lines, were created. *RIOK1* knockdown and re-expression efficiencies were evaluated by western blot (Figure 7A). Confirming our finding in the genomic screen, *RIOK1* knockdown resulted in selective inhibition of the growth of HCT116 *MTAP*$^{-/-}$ cells, with minimal impact on the growth of *MTAPwt* cells (Figure 7B). The growth phenotype was rescued by the expression of shRNA-resistant WT RIOK1 but not by catalytically inactive

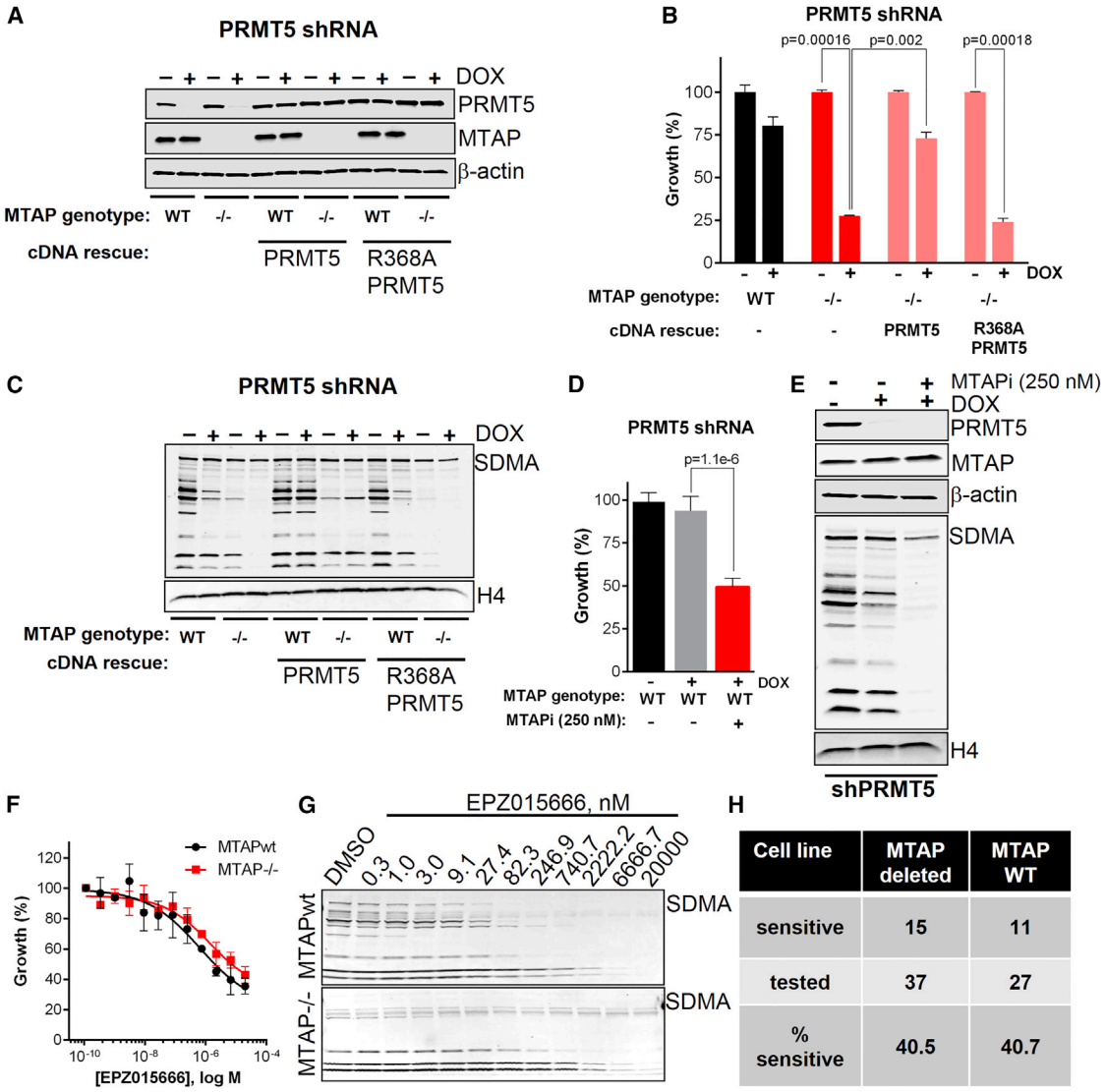

Figure 5. PRMT5 Is Selectively Essential in *MTAP*$^{-/-}$ Cells upon Genetic Ablation but Not Pharmacologic Targeting

(A) Immunoblot analysis of the indicated proteins in the HCT116 isogenic pair stably expressing *PRMT5* shRNA and either p-LVX empty vector control, shRNA-resistant *PRMT5wt* cDNA, or *PRMT5* R368A catalytically dead mutant cDNA.

(B) PRMT5 is selectively essential in *MTAP*$^{-/-}$ cells in vitro. Percent growth of HCT116 *MTAP*$^{-/-}$ and *MTAPwt* cells upon PRMT5 knockdown (+DOX), with or without PRMT5wt or R368A mutant rescue, versus no knockdown (−DOX) control in a 10-day colony growth assay (mean ± SD, n = 3). The p values were calculated using a two-tailed paired t test.

(C) Immunoblot analysis of SDMA marks in the HCT116 isogenic pair stably expressing *PRMT5* shRNA and either p-LVX empty vector control, shRNA-resistant *PRMT5wt* cDNA, or *PRMT5* R368A catalytically dead mutant cDNA.

(D) Percent growth of HCT116 *MTAPwt* cells upon PRMT5 knockdown (+DOX) in a 4-day in vitro growth assay. The experiment was performed in parallel in the absence or presence of the MTA transition state analog inhibitor of MTAP (MTAPi) at 250 nM (mean ± SD, n = 6). The p values were calculated using a two-tailed paired t test.

(E) Immunoblot analysis of the indicated proteins in HCT116 *MTAPwt* cells stably expressing *PRMT5* shRNA upon PRMT5 knockdown (+DOX) or co-treatment with MTAPi.

(F) Dose-response analysis with EPZ015666 titrated from a 20 μM top dose in HCT116 *MTAPwt* versus *MTAP*$^{-/-}$ cells (mean ± SD, n = 3).

(G) Immunoblot analysis of PRMT5-dependent SDMA marks in the HCT116 isogenic cell line pair treated with indicated doses of EPZ015666 for 5 days.

(H) Analysis of EPZ015666 sensitivity in a cell line panel. Dose-response curves were generated for each cell line, and absolute inhibitor concentration 50 (IC50) for EPZ015666 was determined and used as a measure of sensitivity (20 μM cutoff).

K208R/D324N mutant RIOK1 (Figure 7B). To extend this finding beyond the genetically engineered HCT116 *MTAP*$^{-/-}$ model system, we performed shRNA-mediated knockdown of RIOK1 and PRMT5 in MIAPACA-2 cells, which possess endogenous deletion of the *CDKN2A/MTAP* locus. Depletion of RIOK1 or PRMT5 reduced growth of MIAPACA-2 cells (Figure 7C).

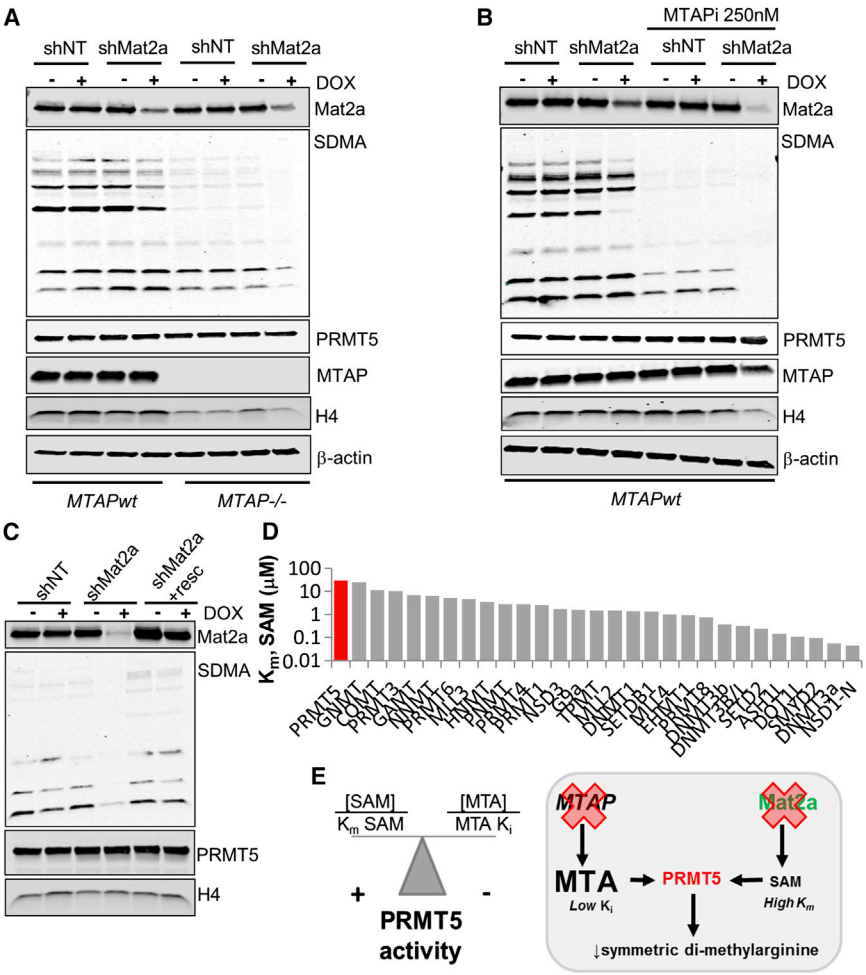

Figure 6. MAT2A Ablation Selectively Inhibits PRMT5 Activity in *MTAP*$^{-/-}$ Cells

(A) Immunoblot analysis of the indicated proteins in the HCT116 isogenic pair stably expressing NT shRNA (shNT) or shMAT2A.

(B) Immunoblot analysis of the indicated proteins in the HCT116 *MTAPwt* cell line stably expressing shNT or shMAT2A in the presence or absence of MTAP inhibitor (250 nM).

(C) Immunoblot analysis of the indicated proteins in the MCF7 cells stably expressing shNT, shMAT2A, and shRNA-resistant *MAT2A* cDNA (shMAT2A+resc). For (A)–(C), DOX (200 ng/ml) was added to induce shMAT2A expression.

(D) SAM Km values (in micromolars) are shown for a panel of methyltransferases analyzed for their sensitivity to MTA.

(E) Schematic depicting convergence of MTAP deficiency-induced metabolic vulnerability due to MTA accumulation and reduced levels of SAM upon MAT2A ablation on PRMT5, resulting in reduced PRMT5 function in a *MTAP*-deleted, SAM-deprived environment.

Depletion of these target proteins upon induction of shRNA expression was confirmed by western blot (Figure 7D). These data demonstrate that the metabolic vulnerability arising upon accumulation of MTA in an MTAP-deficient background extends downstream of PRMT5 and affects PRMT5 binding partner RIOK1.

PRMT5 participates in several multimeric protein co-complexes, including the obligatory binding partner WD45/MEP50 (Wilczek et al., 2011), the mutually exclusive partners pICln and RIOK1 (Guderian et al., 2011), and the nuclear regulator of specificity COPR5 (co-operator of PRMT5) (Lacroix et al., 2008). MEP50, pICln, and COPR5 were not represented in the shRNA library used in our initial screen (Figures 1B–1F); thus, the screen did not provide data indicating whether the MTAP synthetic lethality is shared by other PRMT5 co-complex members or is unique to RIOK1. To determine whether the vulnerability of MTAP-deficient cells extends to PRMT5 co-complexes beyond the RIOK1 co-complex, we performed siRNA pool-mediated knockdown of multiple PRMT5 co-complex members, including PRMT5, RIOK1, MEP50, pICln, and COPR5, in the HCT116 isogenic pair (Figures 7E and S7A). We observed selective inhibition of the growth of MTAP-deficient cells upon knockdown of each PRMT5 co-complex partner (Figure 7E). We assessed PRMT5 protein levels following knockdown of each of these proteins (Figure S7B) and observed that MEP50 knockdown led to a reduction in PRMT5 levels, while knockdown of RIOK1, pICln, or COPR5 did not. Thus, reduction in PRMT5 levels secondary to knockdown of these proteins is not sufficient to explain the MTAP-selective growth inhibition. These data suggest that vulnerability of MTAP-deficient cells is not restricted to the RIOK1 co-complex but rather is broad, affecting several co-complexes involving PRMT5 as a binding partner. Knockdown of these PRMT5 co-complex members led to differential effects on SDMA marks, demonstrating that these proteins constitute different PRMT5 co-complexes (Figure S7C).

DISCUSSION

The mammalian metabolome is characterized by a high degree of flexibility and redundancy (Thiele et al., 2013). MTA is thus unusual in that it is consumed by a solitary, non-redundant enzyme, MTAP. We observed that upon *MTAP* deletion, MTA accumulates to an intracellular concentration of approximately 100 μM, and cells begin to excrete excess MTA. This accumulation of MTA led to an unexpected collateral vulnerability in the arginine methyltransferase PRMT5. While the shRNA library contained 39 methyltransferases, PRMT5 was unique in its high degree of *MTAP* selectivity. Biochemical profiling of methyltransferases revealed a molecular basis for this phenomenon. Among the 33 methyltransferases that we tested in vitro, PRMT5 was the enzyme most sensitive to inhibition by MTA. In vitro inhibition of PRMT5 by MTA occurs at concentrations similar to those

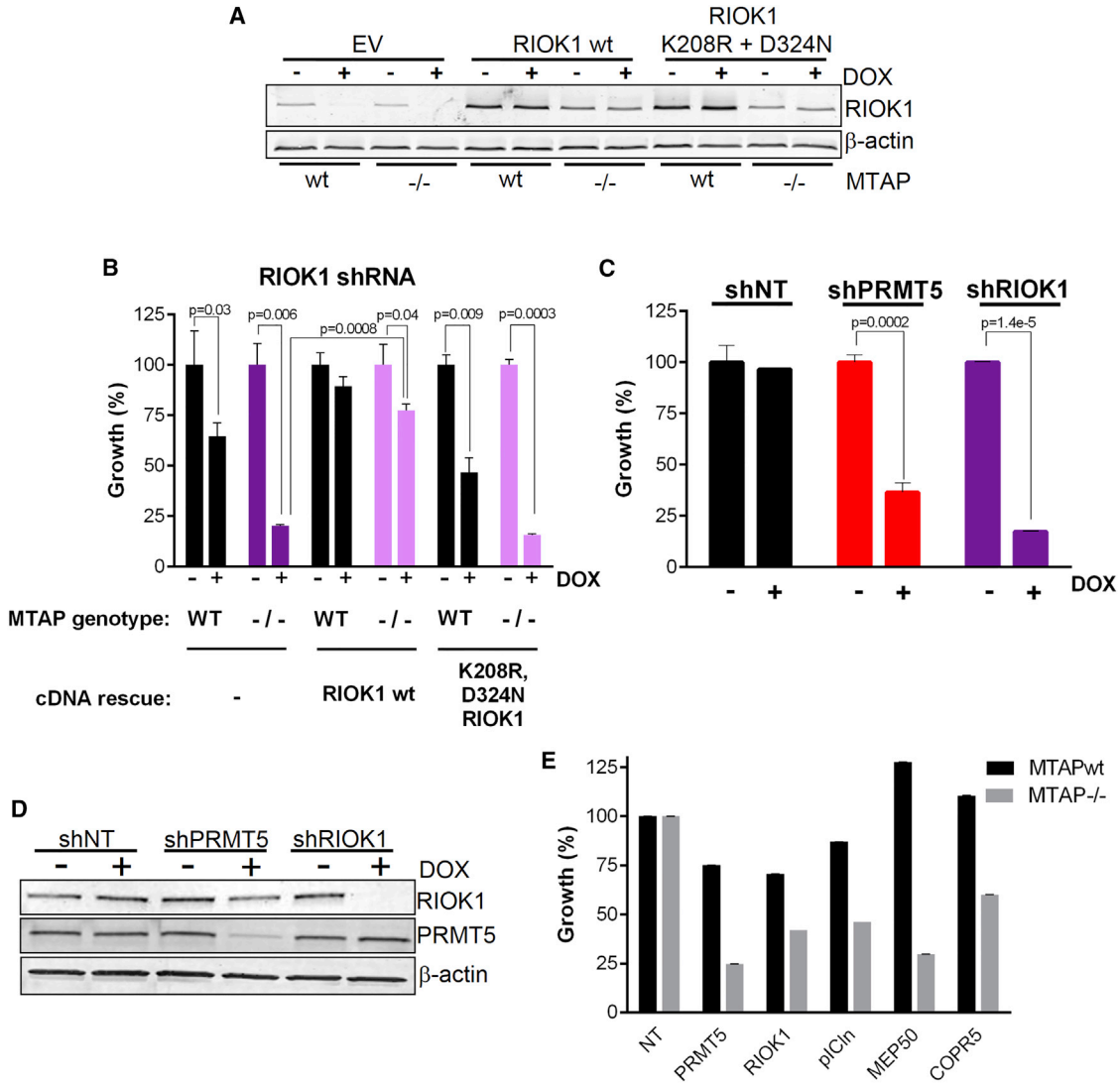

Figure 7. Multiple PRMT5 Co-complexes Are Vulnerable in *MTAP*$^{-/-}$ Cells

(A) Immunoblot analysis of the indicated proteins in the HCT116 isogenic pair stably expressing *RIOK1* shRNA and empty vector control (EV), *RIOK1* shRNA and shRNA-resistant *RIOK1wt* cDNA (RIOK1wt), or *RIOK1* K208R/D324N catalytically dead mutant cDNA. DOX (200 ng/ml) was added to induce shRNA expression.

(B) Percent growth of HCT116 *MTAP*$^{-/-}$ and *MTAPwt* cells upon RIOK1 knockdown (+DOX), with or without RIOK1wt or RIOK1 K208R/D324N mutant rescue, versus no knockdown (−DOX) control in a 10-day colony growth assay (mean ± SD, n = 3).

(C) Percent growth of MIAPACA-2 *MTAP*-deleted cells upon PRMT5 or RIOK1 knockdown (+DOX) in a 10-day colony growth assay (mean ± SD, n = 3).

(D) Immunoblot analysis of the indicated proteins in MIAPACA-2 cells stably expressing *PRMT5* or *RIOK1* shRNA. DOX (200 ng/ml) was added to induce shRNA expression.

(E) Percent growth of *MTAP*$^{-/-}$ and *MTAPwt* cells upon transfection with NT siRNA or siRNA targeting PRMT5, RIOK1, pICln, MEP50, or COPR5 as measured in a 4-day growth assay. (mean ± SD, n = 5). All p values were calculated using a two-tailed paired t test.

observed in *MTAP*-deleted cells, suggesting that this is a biologically relevant phenomenon. We observed substantially reduced basal levels of PRMT5 methyl marks in cells with *MTAP* deletion. Reduced basal PRMT5 activity creates a vulnerability to further ablation of PRMT5 by shRNA. Consistent with our findings, large-scale shRNA screening of broad panels of cancer cell lines has identified the collateral vulnerability to PRMT5 suppression that arises in cancer cell lines with *MTAP* deletion (Kryukov et al., 2016; Mavrakis et al., 2016). These large-scale screening efforts demonstrate that the collateral vulnerability to PRMT5 persists in many *MTAP*-null cancer cell lines and thus are complementary with our work in *MTAP* isogenic cells. In addition, we show that the collateral vulnerability extends to the upstream metabolic enzyme MAT2A, as well as to downstream PRMT5 co-complex members such as RIOK1. Thus, these three enzymes constitute a vulnerable axis in *MTAP*-deleted cells.

Treatment with PRMT5 inhibitor EPZ015666 did not lead to selective growth inhibition in *MTAP*-deleted cells. There are

several possible explanations for this disconnect between pharmacologic inhibition and genetic knockdown of PRMT5. First, a kinetic difference in time required to ablate PRMT5 activity could lead to a different cellular outcome between small molecule inhibitor and shRNA-mediated knockdown. Second, it is possible that a subset of cellular PRMT5 is not accessible to inhibition by EPZ015666. This could arise if a PRMT5 binding partner were to occlude the EPZ015666 binding site on PRMT5. Such a phenomenon could serve to protect a pool of PRMT5 enzyme molecules. Lastly, it is possible that the mode of inhibition of PRMT5 by EPZ015666 negatively affects EPZ015666 inhibition of PRMT5 in high-MTA settings. EPZ015666 binds selectively to the SAM-PRMT5 complex via a cation-pi molecular interaction (Chan-Penebre et al., 2015) that is not possible with the MTA-PRMT5 complex. Thus, EPZ015666 cannot bind efficiently to the MTA-PRMT5 complex. Studies with other inhibitor families, such as G-protein coupled receptors, have noted that two inhibitors of a single enzyme can only be synergistic if they bind to separate binding sites and their interaction with target is not mutually exclusive (Breitinger, 2012). We predict that EPZ015666 is not synergistic with MTA and hypothesize that exploiting the PRMT5 vulnerability in *MTAP*-deleted cancers may require the development of MTA-selective PRMT5 inhibitors that bind to the MTA-bound form of PRMT5 and trap the enzyme in that state. MTA-selective inhibitors might afford a greater therapeutic window than that afforded by non-selective inhibitors, because MTAP expression in normal tissues should provide a protective effect by maintaining low MTA levels. Mouse genetic studies have revealed that PRMT5 has important roles in normal physiology; PRMT5 knockout leads to embryonic lethality (Tee et al., 2010), and substantial toxicities arise upon tissue-specific PRMT5 knockout in the CNS (Bezzi et al., 2013), skeletal muscle (Zhang et al., 2015), and hematopoietic lineages (Liu et al., 2015). These toxicities may become dose limiting in the clinical setting, narrowing the therapeutic potential of agents that non-selectively target PRMT5.

Cellular methyltransferase activity is subject to regulatory control by small molecule metabolites. It has previously been established that methyltransferases are regulated by the relative balance of substrate SAM and product S-adenosylhomocysteine (SAH) (Vance et al., 1997). The SAM/SAH ratio is used to calculate cellular "methylation potential" as a measure of cellular poise to conduct methyltransferase reactions (Williams and Schalinske, 2007). Our observation that PRMT5 can be inhibited by MTA implicates PRMT5 as the exemplar member of a biochemically distinct family of methyltransferases that can be regulated by the SAM/MTA ratio. This regulatory mode is revealed clearly in *MTAP*-deleted cancer cells, where MTA levels accumulate dramatically. Limited information is available regarding MTA levels across normal tissues (Stevens et al., 2010), and wider MTA screening might reveal other settings in which MTA accumulation leads to inhibition of PRMT5. In addition, PRMT5 has a fairly weak binding affinity for SAM. This is unusual among the methyltransferase family, because most mammalian methyltransferases have SAM Km values 10- to 100-fold below its physiologic concentration (Richon et al., 2011). This biochemical finding implies that PRMT5 is poised as a SAM-sensitive methyltransferase, and this sensitivity is exemplified by the reduction in PRMT5 methyl marks that is observed upon MAT2A depletion in *MTAP*-deleted cells.

PRMT5 activity may be mechanistically connected to MAT2A activity through both the relatively poor affinity of PRMT5 for SAM and its high affinity for MTA, as well as the SAM-competitive nature of MTA-mediated inhibition. In cells with active MTAP, MTA concentrations are low, and the ratio of the cellular concentration of SAM in comparison to the Km for SAM is higher than the ratio of the concentration of MTA to the Ki for MTA; the PRMT5 enzyme is active as the PRMT5:SAM form is favored (Figure 6E). In the metabolically altered, high-MTA environment of MTAP-deficient cells, the ratio of the cellular concentration of MTA to the Ki for MTA is increased compared to WT cells; PRMT5 activity is more sensitive to decreases in the cellular concentration of SAM. Reduction in SAM concentration due to knockdown of the SAM-producing MAT2A enzyme further tilts the equilibrium between the active PRMT5:SAM and the inactive PRMT5:MTA complexes toward the inactive form, resulting in a global decrease in PRMT5 activity.

PRMT5 regulates a number of proliferative and biosynthetic processes, such as histone methylation that controls expression of cell-cycle genes (Chung et al., 2013), methylation of growth factor signaling components like EGFR and Raf (Andreu-Pérez et al., 2011; Hsu et al., 2011), and methylation of key protein components required for maturation of ribosome and spliceosome complexes (Friesen et al., 2001; Ren et al., 2010). Thus, PRMT5 activity leads to coordinated upregulation of a range of pro-proliferative and biosynthetic pathways. PRMT5 has been demonstrated to be important for proliferation in tumor models in vivo (Gu et al., 2012; Yan et al., 2014). The tumor models used in these studies happen to carry endogenous deletion of the *CDKN2A/MTAP* locus. PRMT5 is an attractive therapeutic target, and our work suggests that inhibitors that could trap PRMT5 in the MTA-bound state may have particularly robust therapeutic window in *CDKN2A/MTAP*-deleted tumors.

The vulnerability of PRMT5 in MTAP-deficient cancers extends both upstream of PRMT5 (to MAT2A) and downstream of PRMT5 (to RIOK1 and other PRMT5 co-complex members). Thus, in addition to the potential to devise MTA-selective PRMT5 inhibitors, our work demonstrates that therapeutic targeting of MAT2A, RIOK1, or other PRMT5 co-complex members could selectively affect *MTAP*-deleted cancers while sparing MTAP-expressing normal tissues. Using catalytically dead point mutants of RIOK1, we demonstrate that catalytic activity of the enzyme is critical, indicating that pharmacologic inhibitors of RIOK1 may selectively block growth of MTAP-deficient cancers. Thus, this vulnerable axis merits further consideration for therapeutic targeting to address the unmet clinical need in ~15% of human cancers with deletion of the *CDKN2A/MTAP* locus. In addition, these collateral vulnerabilities of MTAP-deficient cancers exemplify an extensible approach to target tumor suppressor loss of function by identification of synthetic lethal relationships with co-deleted metabolic genes.

EXPERIMENTAL PROCEDURES

Cell Lines

HCT116 colon carcinoma *MTAPwt* cells and the *MTAP*$^{-/-}$ isogenic clone were licensed from Horizon Discovery. All other cell lines were obtained from the

American Type Culture Collection, RIKEN Bioresource Center cell bank, or Deutsche Sammlung von Mikroorganismen und Zellkulturen (DSMZ).

shRNA-Based Genomic Screen

See Supplemental Experimental Procedures for a detailed description of the shRNA screen and data analysis.

Generation of Stable Inducible shRNA and cDNA Rescue Cell Lines

All shRNAs constructs were cloned into the pLKO-Tet-on lentiviral backbone vector (Wiederschain et al., 2009) or pSLIK-Tet-on vector. *MTAP*, *PRMT5*, *MAT2A*, *RIOK1* WT, and catalytically dead mutant cDNAs were cloned into pLVX-IRES-neo/puro/blast lentiviral vector. See Supplemental Experimental Procedures for shRNA sequences and additional details.

siRNA Transfections

Cells were transfected with ON-Target plus SMARTpool siRNAs (Dharmacon) using Lipofectamine RNAiMAX (13778-150, Life Technologies) per vendor protocol. To ensure robust and durable knockdown of the target, two sequential transfections were performed, separated by 24 hr of recovery in full growth media (RPMI + 10% fetal bovine serum). At 24 hr after the second transfection, cells were trypsinized, counted, and plated for 96-well format growth assays.

Growth Assays

Following siRNA transfection or 4-day pre-treatment with 200 ng/ml DOX as relevant, cells were plated in 96-well tissue culture plates at 1,000 to 3,000 cells per well. CellTiter-Glo ATP assay (Promega) was performed on parallel assay plates at t_0 and at the end of the cell culture period as indicated in figure legends. Percent growth was calculated as either percent change in the luminescence readout for the experimental condition at the end of the assay, compared to that of NT hairpin control in the absence of DOX, or as percent change in the t_{end}/t_0 luminescence readout normalized to that of NT or Luc hairpin control in the presence of DOX.

For colony formation assays, cells were plated at 1,000 per well in a 6-well plate and DOX treatment (200 ng/ml) was initiated at the time of plating using an equivalent volume of sterile water as vehicle control. Colonies were fixed after 10 days and stained with 0.05% crystal violet in 4.5% paraformaldehyde solution for 24 hr. Colonies were quantified using LI-COR image processing software (LI-COR Biosciences).

Immunoblotting

Antibodies used in immunoblotting are listed in Supplemental Experimental Procedures.

PRMT5 Inhibitor

PRMT5 inhibitor EPZ015666 was synthesized following the published synthetic protocol (Chan-Penebre et al., 2015).

N-Methyltransferase In Vitro Activity Assays

In vitro screening of methyltransferase inhibition by MTA, as well as SAM Km measurements, was conducted using a panel of standard methyltransferase assays at Eurofins CEREP Panlabs. Additional information regarding assay methods and in vitro assay data analysis can be found in Supplemental Experimental Procedures.

Metabolite Extraction and LC-MS Analysis

For media analysis, conditioned media were collected from cells that were cultured for at least 24 hr and diluted 20-fold before LC-MS analysis. For intracellular metabolites, organic extraction was performed with cold 80%/20% (v/v) methanol/water with d^8-putrescine added as an internal standard following normalization to cell number. Samples were then dried under reduced pressure and stored at −80°C until LC-MS analysis. See Supplemental Experimental Procedures for additional details regarding sample processing, LC-MS, and data analysis.

Xenograft Studies

See Supplemental Experimental Procedures.

SUPPLEMENTAL INFORMATION

Supplemental Information includes Supplemental Experimental Procedures, seven figures, and three tables and can be found with this article online at http://dx.doi.org/10.1016/j.celrep.2016.03.043.

AUTHOR CONTRIBUTIONS

K.M. and K.M.M. wrote the manuscript; M.J.C., P.Q., M.F.C., E.M., M.M., K.K., and S.G. conducted experiments; K.M., S.C., A.K., S.G., Z.K., M.L.B., J.M., and K.M.M. conceived experiments and analyzed data; J.T. provided reagents; and M.D. and S.A.B. provided expertise and feedback.

ACKNOWLEDGMENTS

We thank Manilduth Ramnath and colleagues at Eurofins CEREP Panlabs for providing information and sharing expertise regarding methyltransferase enzymology and Victor De Jesus, Sheila Newhouse, and Rob Silva for support with animal husbandry and in vivo studies. We thank also Andrew Olaharski and Amelia Barnett for helpful suggestions and critical review of the manuscript and Helen Varley for formatting and editorial assistance.

Received: December 9, 2015
Revised: February 8, 2016
Accepted: March 10, 2016
Published: April 7, 2016

REFERENCES

Andreu-Pérez, P., Esteve-Puig, R., de Torre-Minguela, C., López-Fauqued, M., Bech-Serra, J.J., Tenbaum, S., García-Trevijano, E.R., Canals, F., Merlino, G., Avila, M.A., and Recio, J.A. (2011). Protein arginine methyltransferase 5 regulates ERK1/2 signal transduction amplitude and cell fate through CRAF. Sci. Signal. *4*, ra58.

Angermayr, M., Roidl, A., and Bandlow, W. (2002). Yeast Rio1p is the founding member of a novel subfamily of protein serine kinases involved in the control of cell cycle progression. Mol. Microbiol. *44*, 309–324.

Antonysamy, S., Bonday, Z., Campbell, R.M., Doyle, B., Druzina, Z., Gheyi, T., Han, B., Jungheim, L.N., Qian, Y., Rauch, C., et al. (2012). Crystal structure of the human PRMT5:MEP50 complex. Proc. Natl. Acad. Sci. USA *109*, 17960–17965.

Arrowsmith, C.H., Bountra, C., Fish, P.V., Lee, K., and Schapira, M. (2012). Epigenetic protein families: a new frontier for drug discovery. Nat. Rev. Drug Discov. *11*, 384–400.

Basu, I., Locker, J., Cassera, M.B., Belbin, T.J., Merino, E.F., Dong, X., Hemeon, I., Evans, G.B., Guha, C., and Schramm, V.L. (2011). Growth and metastases of human lung cancer are inhibited in mouse xenografts by a transition state analogue of 5'-methylthioadenosine phosphorylase. J. Biol. Chem. *286*, 4902–4911.

Beroukhim, R., Mermel, C.H., Porter, D., Wei, G., Raychaudhuri, S., Donovan, J., Barretina, J., Boehm, J.S., Dobson, J., Urashima, M., et al. (2010). The landscape of somatic copy-number alteration across human cancers. Nature *463*, 899–905.

Bezzi, M., Teo, S.X., Muller, J., Mok, W.C., Sahu, S.K., Vardy, L.A., Bonday, Z.Q., and Guccione, E. (2013). Regulation of constitutive and alternative splicing by PRMT5 reveals a role for Mdm4 pre-mRNA in sensing defects in the spliceosomal machinery. Genes Dev. *27*, 1903–1916.

Breitinger, H.-G. (2012). Drug synergy—mechanisms and methods of analysis. In Toxicity and Drug Testing, W. Acree, ed. (InTech). http://www.intechopen.com/books/toxicity-and-drug-testing/drug-synergy-mechanisms-and-methods-of-analysis.

Chan-Penebre, E., Kuplast, K.G., Majer, C.R., Boriack-Sjodin, P.A., Wigle, T.J., Johnston, L.D., Rioux, N., Munchhof, M.J., Jin, L., Jacques, S.L., et al. (2015). A selective inhibitor of PRMT5 with in vivo and in vitro potency in MCL models. Nat. Chem. Biol. *11*, 432–437.

Chilcote, R.R., Brown, E., and Rowley, J.D. (1985). Lymphoblastic leukemia with lymphomatous features associated with abnormalities of the short arm of chromosome 9. N. Engl. J. Med. *313*, 286–291.

Chung, J., Karkhanis, V., Tae, S., Yan, F., Smith, P., Ayers, L.W., Agostinelli, C., Pileri, S., Denis, G.V., Baiocchi, R.A., and Sif, S. (2013). Protein arginine methyltransferase 5 (PRMT5) inhibition induces lymphoma cell death through reactivation of the retinoblastoma tumor suppressor pathway and polycomb repressor complex 2 (PRC2) silencing. J. Biol. Chem. *288*, 35534–35547.

Enouf, J., Lawrence, F., Tempete, C., Robert-Gero, M., and Lederer, E. (1979). Relationship between inhibition of protein methylase I and inhibition of Rous sarcoma virus-induced cell transformation. Cancer Res. *39*, 4497–4502.

Frezza, C., Zheng, L., Folger, O., Rajagopalan, K.N., MacKenzie, E.D., Jerby, L., Micaroni, M., Chaneton, B., Adam, J., Hedley, A., et al. (2011). Haem oxygenase is synthetically lethal with the tumour suppressor fumarate hydratase. Nature *477*, 225–228.

Friesen, W.J., Paushkin, S., Wyce, A., Massenet, S., Pesiridis, G.S., Van Duyne, G., Rappsilber, J., Mann, M., and Dreyfuss, G. (2001). The methylosome, a 20S complex containing JBP1 and pICln, produces dimethylarginine-modified Sm proteins. Mol. Cell. Biol. *21*, 8289–8300.

Gu, Z., Gao, S., Zhang, F., Wang, Z., Ma, W., Davis, R.E., and Wang, Z. (2012). Protein arginine methyltransferase 5 is essential for growth of lung cancer cells. Biochem. J. *446*, 235–241.

Guderian, G., Peter, C., Wiesner, J., Sickmann, A., Schulze-Osthoff, K., Fischer, U., and Grimmler, M. (2011). RioK1, a new interactor of protein arginine methyltransferase 5 (PRMT5), competes with pICln for binding and modulates PRMT5 complex composition and substrate specificity. J. Biol. Chem. *286*, 1976–1986.

Hsu, J.M., Chen, C.T., Chou, C.K., Kuo, H.P., Li, L.Y., Lin, C.Y., Lee, H.J., Wang, Y.N., Liu, M., Liao, H.W., et al. (2011). Crosstalk between Arg 1175 methylation and Tyr 1173 phosphorylation negatively modulates EGFR-mediated ERK activation. Nat. Cell Biol. *13*, 174–181.

Kamijo, T., Zindy, F., Roussel, M.F., Quelle, D.E., Downing, J.R., Ashmun, R.A., Grosveld, G., and Sherr, C.J. (1997). Tumor suppression at the mouse INK4a locus mediated by the alternative reading frame product p19ARF. Cell *91*, 649–659.

Kryukov, G.V., Wilson, F.H., Ruth, J.R., Paulk, J., Tsherniak, A., Marlow, S.E., Vazquez, F., Weir, B.A., Fitzgerald, M.E., Tanaka, M., et al. (2016). MTAP deletion confers enhanced dependency on the PRMT5 arginine methyltransferase in cancer cells. Science *351*, 1214–1218.

Lacroix, M., El Messaoudi, S., Rodier, G., Le Cam, A., Sardet, C., and Fabbrizio, E. (2008). The histone-binding protein COPR5 is required for nuclear functions of the protein arginine methyltransferase PRMT5. EMBO Rep. *9*, 452–458.

Li, W., Su, D., Mizobuchi, H., Martin, D.S., Gu, B., Gorlick, R., Cole, P., and Bertino, J.R. (2004). Status of methylthioadenosine phosphorylase and its impact on cellular response to L-alanosine and methylmercaptopurine riboside in human soft tissue sarcoma cells. Oncol. Res. *14*, 373–379.

Liu, F., Cheng, G., Hamard, P.J., Greenblatt, S., Wang, L., Man, N., Perna, F., Xu, H., Tadi, M., Luciani, L., and Nimer, S.D. (2015). Arginine methyltransferase PRMT5 is essential for sustaining normal adult hematopoiesis. J. Clin. Invest. *125*, 3532–3544.

Longshaw, A.I., Adanitsch, F., Gutierrez, J.A., Evans, G.B., Tyler, P.C., and Schramm, V.L. (2010). Design and synthesis of potent "sulfur-free" transition state analogue inhibitors of 5'-methylthioadenosine nucleosidase and 5'-methylthioadenosine phosphorylase. J. Med. Chem. *53*, 6730–6746.

Lord, C.J., Tutt, A.N., and Ashworth, A. (2015). Synthetic lethality and cancer therapy: lessons learned from the development of PARP inhibitors. Annu. Rev. Med. *66*, 455–470.

Mavrakis, K.J., McDonald, E.R., 3rd, Schlabach, M.R., Billy, E., Hoffman, G.R., deWeck, A., Ruddy, D.A., Venkatesan, K., Yu, J., McAllister, G., et al. (2016). Disordered methionine metabolism in MTAP/CDKN2A-deleted cancers leads to dependence on PRMT5. Science *351*, 1208–1213.

Meister, G., Eggert, C., Bühler, D., Brahms, H., Kambach, C., and Fischer, U. (2001). Methylation of Sm proteins by a complex containing PRMT5 and the putative U snRNP assembly factor pICln. Curr. Biol. *11*, 1990–1994.

Muller, F.L., Colla, S., Aquilanti, E., Manzo, V.E., Genovese, G., Lee, J., Eisenson, D., Narurkar, R., Deng, P., Nezi, L., et al. (2012). Passenger deletions generate therapeutic vulnerabilities in cancer. Nature *488*, 337–342.

Muller, F.L., Aquilanti, E.A., and DePinho, R.A. (2015). Collateral lethality: a new therapeutic strategy in oncology. Trends Cancer *1*, 161–173.

Pagliarini, D.J., Calvo, S.E., Chang, B., Sheth, S.A., Vafai, S.B., Ong, S.E., Walford, G.A., Sugiana, C., Boneh, A., Chen, W.K., et al. (2008). A mitochondrial protein compendium elucidates complex I disease biology. Cell *134*, 112–123.

Parsons, D.W., Jones, S., Zhang, X., Lin, J.C., Leary, R.J., Angenendt, P., Mankoo, P., Carter, H., Siu, I.M., Gallia, G.L., et al. (2008). An integrated genomic analysis of human glioblastoma multiforme. Science *321*, 1807–1812.

Pesiridis, G.S., Diamond, E., and Van Duyne, G.D. (2009). Role of pICLn in methylation of Sm proteins by PRMT5. J. Biol. Chem. *284*, 21347–21359.

Pollack, B.P., Kotenko, S.V., He, W., Izotova, L.S., Barnoski, B.L., and Pestka, S. (1999). The human homologue of the yeast proteins Skb1 and Hsl7p interacts with Jak kinases and contains protein methyltransferase activity. J. Biol. Chem. *274*, 31531–31542.

Ren, J., Wang, Y., Liang, Y., Zhang, Y., Bao, S., and Xu, Z. (2010). Methylation of ribosomal protein S10 by protein-arginine methyltransferase 5 regulates ribosome biogenesis. J. Biol. Chem. *285*, 12695–12705.

Richon, V.M., Johnston, D., Sneeringer, C.J., Jin, L., Majer, C.R., Elliston, K., Jerva, L.F., Scott, M.P., and Copeland, R.A. (2011). Chemogenetic analysis of human protein methyltransferases. Chem. Biol. Drug Des. *78*, 199–210.

Ruefli-Brasse, A., Sakamoto, D., Orf, J., Rong, M., Shi, J., Carlson, T., Quon, K., Kamb, A., and Wickramasinghe, D. (2011). Methylthioadenosine (MTA) rescues methylthioadenosine phosphorylase (MTAP)-deficient tumors from purine synthesis inhibition in vivo via non-autonomous adenine supply. J. Cancer Ther. *2*, 523–534.

Serrano, M., Hannon, G.J., and Beach, D. (1993). A new regulatory motif in cell--cycle control causing specific inhibition of cyclin D/CDK4. Nature *366*, 704–707.

Stevens, A.P., Dettmer, K., Kirovski, G., Samejima, K., Hellerbrand, C., Bosserhoff, A.K., and Oefner, P.J. (2010). Quantification of intermediates of the methionine and polyamine metabolism by liquid chromatography-tandem mass spectrometry in cultured tumor cells and liver biopsies. J. Chromatogr. A *1217*, 3282–3288.

Sun, L., Wang, M., Lv, Z., Yang, N., Liu, Y., Bao, S., Gong, W., and Xu, R.M. (2011). Structural insights into protein arginine symmetric dimethylation by PRMT5. Proc. Natl. Acad. Sci. USA *108*, 20538–20543.

Tee, W.W., Pardo, M., Theunissen, T.W., Yu, L., Choudhary, J.S., Hajkova, P., and Surani, M.A. (2010). Prmt5 is essential for early mouse development and acts in the cytoplasm to maintain ES cell pluripotency. Genes Dev. *24*, 2772–2777.

Thiele, I., Swainston, N., Fleming, R.M., Hoppe, A., Sahoo, S., Aurich, M.K., Haraldsdottir, H., Mo, M.L., Rolfsson, O., Stobbe, M.D., et al. (2013). A community-driven global reconstruction of human metabolism. Nat. Biotechnol. *31*, 419–425.

Vance, D.E., Walkey, C.J., and Cui, Z. (1997). Phosphatidylethanolamine N-methyltransferase from liver. Biochim. Biophys. Acta *1348*, 142–150.

Widmann, B., Wandrey, F., Badertscher, L., Wyler, E., Pfannstiel, J., Zemp, I., and Kutay, U. (2012). The kinase activity of human Rio1 is required for final steps of cytoplasmic maturation of 40S subunits. Mol. Biol. Cell *23*, 22–35.

Wiederschain, D., Wee, S., Chen, L., Loo, A., Yang, G., Huang, A., Chen, Y., Caponigro, G., Yao, Y.M., Lengauer, C., et al. (2009). Single-vector inducible lentiviral RNAi system for oncology target validation. Cell Cycle *8*, 498–504.

Wilczek, C., Chitta, R., Woo, E., Shabanowitz, J., Chait, B.T., Hunt, D.F., and Shechter, D. (2011). Protein arginine methyltransferase Prmt5-Mep50 methylates histones H2A and H4 and the histone chaperone nucleoplasmin in *Xenopus laevis* eggs. J. Biol. Chem. *286*, 42221–42231.

Williams, K.T., and Schalinske, K.L. (2007). New insights into the regulation of methyl group and homocysteine metabolism. J. Nutr. *137*, 311–314.

Yan, F., Alinari, L., Lustberg, M.E., Martin, L.K., Cordero-Nieves, H.M., Banasavadi-Siddegowda, Y., Virk, S., Barnholtz-Sloan, J., Bell, E.H., Wojton, J., et al. (2014). Genetic validation of the protein arginine methyltransferase PRMT5 as a candidate therapeutic target in glioblastoma. Cancer Res. *74*, 1752–1765.

Zappia, V., Della Ragione, F., Pontoni, G., Gragnaniello, V., and Cartenì-Farina, M. (1988). Human 5′-deoxy-5′-methylthioadenosine phosphorylase: kinetic studies and catalytic mechanism. Adv. Exp. Med. Biol. *250*, 165–177.

Zhang, H., Chen, Z.H., and Savarese, T.M. (1996). Codeletion of the genes for p16INK4, methylthioadenosine phosphorylase, interferon-alpha1, interferon-beta1, and other 9p21 markers in human malignant cell lines. Cancer Genet. Cytogenet. *86*, 22–28.

Zhang, T., Günther, S., Looso, M., Künne, C., Krüger, M., Kim, J., Zhou, Y., and Braun, T. (2015). Prmt5 is a regulator of muscle stem cell expansion in adult mice. Nat. Commun. *6*, 7140.